




Powder X-ray structural analysis and bandgap measurements for $(\text{Ca}_x\text{Sr}_{2-x})\text{MnWO}_6$ ($x = 0.25, 0.5, 0.75, 1.5, 1.75$)

Winnie Wong-Ng ^{1,a}, Yuqi Yang,² YuCheng Lan,³ Guangyao Liu ⁴, Amrit Kafle,⁵ Weifang Liu,⁶ Jie Hou,¹ Donald Windover,¹ Qing Huang,⁷ Sergiy Krylyuk,¹ and James A. Kaduk ^{8,9}

¹Material Measurement Laboratory, National Institute of Standards and Technology, Gaithersburg, MD 20899, USA

²Institute of Materials Science and Engineering, Sichuan University of Science and Engineering, Zigong 643000, China

³Physics Department, Morgan State University, Baltimore, MD, USA

⁴State Key Laboratory of Geological Processes and Mineral Resources, and Institute of Earth Sciences, China University of Geosciences, Beijing 100083, China

⁵Physics Department, Catholic University, Washington, DC 20064, USA

⁶School of Science, Tianjin University, Tianjin 300072, China

⁷NIST Center for Neutron Research (NCNR), National Institute of Standards and Technology, Gaithersburg, MD 20899, USA

⁸Department of Chemistry, Illinois Institute of Technology, Chicago, IL 60616, USA

⁹Department of Physics, North Central College, Naperville, IL 60540, USA

(Received 24 October 2021; accepted 10 May 2022)

The structure, powder diffraction patterns and bandgap measurements of a series of manganese- and tungsten-containing alkaline-earth double perovskites $(\text{Ca}_x\text{Sr}_{2-x})\text{MnWO}_6$ ($x = 0.25, 0.5, 0.75, 1.5, 1.75$) have been investigated. Powder X-ray diffraction patterns of this series of compounds measured at room temperature have been submitted to be included in the Powder Diffraction File (PDF). These compounds crystallize in monoclinic space group $P2_1/n$ (No.14). From $(\text{Ca}_{1.75}\text{Sr}_{0.25})\text{MnWO}_6$ to $(\text{Ca}_{0.25}\text{Sr}_{1.75})\text{MnWO}_6$, lattice parameters a range from 5.6729(2) Å to 5.6774(4) Å, b from 5.5160(2) Å to 5.6638(4) Å, c from 7.8741(3) Å to 8.0051(4) Å, V from 240.39(2) Å³ to 257.410(12) Å³, and $Z = 2$. These compounds are pseudo-tetragonal. They all consist of distorted MnO_6 and WO_6 octahedra with rotational mismatch angles and tilt angles with respect to each other. For $(\text{Ca}_x\text{Sr}_{2-x})\text{MnWO}_6$, as x increases, the mismatch angles for MnO_6 octahedra increase from 7.96 (6)° to 13.12(8)° and from 9.28(7)° to 14.87(9)° for WO_6 octahedra. Correspondingly, the tilt angles range from 11.60(15)° to 14.20(3)° for MnO_6 , and from 13.34(2)° to 16.35(3)° for WO_6 . Bandgap measurements suggest that these compounds to be direct-allowed semiconductors with bandgaps ranging from 1.5 to 2.5 eV, indicating that members of $(\text{Ca}_x\text{Sr}_{2-x})\text{MnWO}_6$ are potential photocatalysts and photovoltaic materials that absorb visible light of the solar spectrum. © The Author(s), 2022. Published by Cambridge University Press on behalf of International Centre for Diffraction Data. [doi:10.1017/S0885715622000185]

Key words: $(\text{Ca}_x\text{Sr}_{2-x})\text{MnWO}_6$, X-ray powder diffraction reference patterns, crystal structures, bandgap measurements, semiconductors

I. INTRODUCTION

The PEROVSKITE family of materials exhibit a large variety of applications including photovoltaics, sensors, thermoelectrics, batteries, fuel cells, catalysis, lasers, magnets, superconductors, LEDs, and memory devices (RAM). The general chemical formula for perovskite compounds is ABX_3 , where “A” and “B” are two cations, often of very different sizes, and X is an anion (frequently oxygen) that bonds to both cations. The A atoms are generally larger than the B atoms. The ideal cubic structure has the B cation in 6-fold coordination, surrounded by an octahedron of anions, and the A cation in regular 12-fold coordination. The formula ABX_3 can be expanded to double perovskites and complex perovskites. With the possibility of doping, there are even

larger possible combinations of formulae leading to a wealth of rich chemistry and research opportunities.

In recent years, extensive efforts have been conducted on double perovskites in the hope of searching for new technological applications. The double perovskites with a general formula of $\text{A}_2\text{BB}'\text{O}_6$ (where A = alkaline-earth elements, B and B' = Co, Fe, Mn, Ni, Cu, W, Mo, etc.) are known to exhibit a variety of exotic properties including colossal magnetoresistance, high-temperature superconductivity, and half-metallicity (Blasse, 1965; Galasso, 1969; Viola *et al.*, 2003; Zhao *et al.*, 2005; Manoun *et al.*, 2013). A number of these materials are semiconductors with bandgaps feasible for photovoltaic applications. Some also show relatively high power factors P ($P = S^2 \cdot \sigma$, where S is the Seebeck coefficient and σ is electrical conductivity (Tritt, 1996)), therefore they are also potential candidates as thermoelectric materials for energy conversion applications.

In this paper, we are interested in studying the structure and bandgap information of the double perovskite solid

^aAuthor to whom correspondence should be addressed. Electronic mail: winnie.wong-ng@nist.gov

solutions $(\text{Ca}_x\text{Sr}_{2-x})\text{MnWO}_6$. The structural studies were performed using powder X-ray diffraction with the Rietveld refinement technique. The bandgaps of these materials were performed by measuring the UV–visible absorption spectra. As reference powder diffraction patterns are critical for phase analysis, we also prepare the reference patterns for $(\text{Ca}_x\text{Sr}_{2-x})\text{MnWO}_6$, with $x = 0.25, 0.5, 0.75, 1.5, 1.75$. The reference patterns for the $x = 0.0$ and 2.0 compounds already exist in the Powder Diffraction File (PDF) (Gates-Rector and Blanton, 2019) (Sr_2MnWO_6 (PDF 01-078-4158) and Ca_2MnWO_6 (PDF 04-013-0977)).

II. EXPERIMENTAL

A. Sample preparation

$(\text{Ca}_x\text{Sr}_{2-x})\text{MnWO}_6$ ($x = 0, 0.25, 0.5, 0.75, 1.00, 1.25, 1.5, 1.75, 2.0$) samples were prepared by heating a stoichiometric mixture of SrCO_3 , CaCO_3 , MnO_2 , and WO_3 in air first and then in flowing forming gas (5% H_2 , 95% N_2). Samples were weighed out, well-mixed and heat-treated at 750, 875, and 950 °C in air, each for 2 days with intermediate grindings and pelletizings. These samples were subsequently heat-treated at 1000 °C in flowing forming gas for 20 h. The samples were furnace cooled. The phase purity of the beige-colored samples was established by powder X-ray diffraction. The heat-treatment process was repeated until no further changes were detected in the powder X-ray diffraction patterns. A selected subset of these samples ($x = 0.25, 0.5, 0.75, 1.5, 1.75$) were used for structural studies and for preparing reference patterns.

B. Estimation of the composition using X-ray fluorescence

The estimation of the compositions for three samples of varying atomic ratios $\text{Sr}_a\text{Ca}_b\text{Mn}_c\text{W}_d\text{O}_6$ were performed on a Bruker M4 Tornado micro X-ray fluorescence instrument. An Rh X-ray source, set to 50 kV and 100 μA , with a 20 μm mono-capillary was used for excitation (S.N. 2001495). A Bruker XFlash 450 μm thick, Silicon Drift Detector (S.N. 11881_0239) (The purpose of identifying the equipment in this article is to specify the experimental procedure. Such identification does not imply recommendation or endorsement by the National Institute of Standards and Technology.) was used for data collection for the scans. Each spectrum used a mean peak sum of over 10 000 X-ray counts per analyzed element, reducing counting statistics as a source of uncertainty below all other contributions. Analysis was performed using Bruker Quantify version 1.6.0.286 with the standard Spectrum Elements method and calibrated for our instrument (S.N. 6099). For statistical sampling, 20+ independent, 60 second live time measurements were performed, and the variance of the composition derived from these measurements were used for error analysis.

C. X-ray Rietveld refinements and powder reference patterns

Among the samples prepared, the $(\text{Ca}_x\text{Sr}_{2-x})\text{MnWO}_6$ ($x = 0.25, 0.5, 0.75, 1.5, 1.75$) members were packed into 0.3 mm diameter glass capillaries for X-ray diffraction studies.

The X-ray powder diffraction patterns were measured on a PANalytical Empyrean Debye-Scherrer diffractometer equipped with an incident-beam focusing mirror and an X'Celerator detector. The patterns ($1\text{--}100^\circ 2\theta$, 0.0083557° steps, 4 s per step, $1/4^\circ$ divergence slit, 0.02 radian Soller slits) were measured using $\text{MoK}\alpha$ radiation.

The Rietveld refinement technique (Rietveld, 1969) with the software suite GSAS-II (Toby and von Dreele, 2013) was used to determine the structure of $(\text{Ca}_x\text{Sr}_{2-x})\text{MnWO}_6$ ($x = 0.25, 0.5, 0.75, 1.5, 1.75$). Reference patterns were obtained using a Rietveld pattern decomposition technique. The reported peak positions were derived from the extracted integrated intensities, and positions calculated from the lattice parameters. For peaks that cannot be resolved, the intensities are summed, and an intensity-weighted d-spacing is reported.

D. Bandgap measurements

Optical properties of the $(\text{Ca}_x\text{Sr}_{2-x})\text{MnWO}_6$ ($x = 0.0, 0.25, 0.5, 1.00, 1.5, 1.75, 2.0$) compounds were investigated by obtaining the UV–visible absorption spectra. In this series of studies, we also used compounds of $x = 0.0$ and 2.0 to establish the trend. The UV–visible optical absorption spectra were measured using a DU 640 spectrophotometer equipped with tungsten/deuterium sources and an autocollimating quartz crystal prism as a monochromator. The samples were ground and casted onto Scotch tapes. The light passed through the ground sample particles on tapes and the transmittance was recorded by a photodiode detector from 200 to 1300 nm.

III. RESULTS AND DISCUSSION

A. XRD and XRF results

Results of Rietveld refinements for the $(\text{Ca}_x\text{Sr}_{2-x})\text{MnWO}_6$ ($x = 0.25, 0.5, 0.75, 1.5, 1.75$) series are shown in Table I and Figure 1. Table I gives various refinement statistical agreement factors whereas in Figure 1, the observed (crosses), calculated (solid line), and difference XRD patterns (bottom) for $(\text{Ca}_{0.5}\text{Sr}_{1.5})\text{MnWO}_6$ are illustrated; the difference pattern is plotted at the same scale. The row of tick marks indicates the calculated peak positions. Table II lists the lattice parameters while atomic coordinates and displacement parameters are given in Table III. All samples contain a small amount of W (ranging from 1.8% to 3.8%) (Table I). The presence of W was easy to identify but not the other minor phases associated with the presence of W. These phases are likely present in the amorphous form. As a result, we do not expect a significant deficiency of W in the main phase and therefore affecting the main chemistry. The bond distances are summarized in Table IV.

TABLE I. Rietveld refinement residuals for $(\text{Ca}_x\text{Sr}_{2-x})\text{MnWO}_6$ ($x = 0.25, 0.5, 0.75, 1.5, 1.75$).

Composition	R_{wp}	R_{p}	χ^2	Impurity phase (W, wt%)
$(\text{Ca}_{0.25}\text{Sr}_{1.75})\text{MnWO}_6$	0.0398	0.0311	1.15	1.9
$(\text{Ca}_{0.50}\text{Sr}_{1.50})\text{MnWO}_6$	0.0399	0.0314	1.26	3.1
$(\text{Ca}_{0.75}\text{Sr}_{1.25})\text{MnWO}_6$	0.0428	0.0331	1.24	1.8
$(\text{Ca}_{1.50}\text{Sr}_{0.50})\text{MnWO}_6$	0.0613	0.0482	1.79	3.5
$(\text{Ca}_{1.75}\text{Sr}_{0.25})\text{MnWO}_6$	0.0654	0.0481	1.97	3.8

The structure is monoclinic $P2_1/n$ (No. 14).

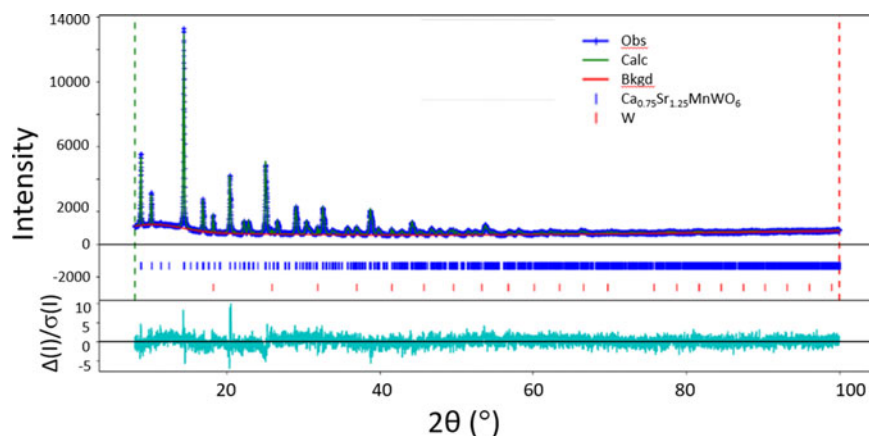


Figure 1. Observed (crosses), calculated (solid line), and difference XRD patterns (bottom) for the powder X-ray diffraction pattern of $(\text{Ca}_{1.25}\text{Sr}_{0.75})\text{MnWO}_6$ by the Rietveld analysis technique. The difference pattern is plotted at the same scale as the other calculated peak positions.

TABLE II. Cell parameters for $(\text{Ca}_x\text{Sr}_{2-x})\text{MnWO}_6$ ($x = 0.25, 0.5, 0.75, 1.5, 1.75$).

Chemical formula	a (Å)	b (Å)	c (Å)	β (°)	V (Å ³)	d_{cal} (g cm ⁻³)	Ref.
$(\text{Ca}_{0.25}\text{Sr}_{1.75})\text{MnWO}_6$	5.6774(4)	5.6638(4)	8.0051(4)	90.062(15)	257.410(12)	6.450	This work
$(\text{Ca}_{0.50}\text{Sr}_{1.50})\text{MnWO}_6$	5.6725(2)	5.6460(3)	7.9890(3)	89.949(13)	255.862(12)	6.326	This work
$(\text{Ca}_{0.75}\text{Sr}_{1.25})\text{MnWO}_6$	5.6662(2)	5.6327(2)	7.9850(4)	90.029(15)	254.849(15)	6.221	This work
$(\text{Ca}_{1.00}\text{Sr}_{1.00})\text{MnWO}_6$	5.651	5.574	7.923	90.17	249.57	—	00-58-706
$(\text{Ca}_{1.25}\text{Sr}_{0.75})\text{MnWO}_6$	5.666	5.574	7.927	90.14	250.35	5.977	00-71-216
$(\text{Ca}_{1.50}\text{Sr}_{0.50})\text{MnWO}_6$	5.6637(2)	5.5412(2)	7.8934(3)	89.07(8)	243.721(11)	5.905	This work
$(\text{Ca}_{1.75}\text{Sr}_{0.25})\text{MnWO}_6$	5.6729(2)	5.5160(2)	7.8741(3)	89.059(8)	240.39(2)	5.747	This work
Ca_2MnWO_6	5.6545	5.4618	7.5022	90.19	240.96	—	4-010-5147

The structure is monoclinic $P2_1/n$ (No. 14), $Z = 2$. The cell volume decreases as the concentration of Ca increases due to the smaller ionic radius of Ca^{2+} compared with Sr^{2+} . The cell parameters of other pertinent phases from the PDF (Gates-Rector and Blanton, 2019) are added.

The atomic ratio calculation for Sr/Mn, Ca/Mn, W/Mn, as well as uncertainties are estimated for each of the three samples using an X-ray fluorescence technique and compared to the provided nominal values (Table V). We assume that Mn is an atomic ratio of “1.0” in this calculation. The Mn was chosen, due to its atomic ratio being a constant for each sample. Expanded uncertainties are provided as ranges for approximate 95% confidence (with a coverage factor of $k = 2$).

The results show a trend agreement in Sr atomic concentrations with two of the three samples agreeing within confidence intervals. In all cases, the Sr ratio is slightly higher than predicted in XRD. The results also show a trend agreement for Ca atomic composition, when compared with XRD results. In each sample, the XRF Ca atomic ratio uncertainty range is slightly below the XRD predicted result. The W atomic concentration from XRF calculated uncertainty ranges shows agreement for two of the three samples, with a slightly higher atomic concentration for the $\text{Sr}_{1.75}\text{Ca}_{0.25}\text{MnWO}_6$ sample. The slightly higher W atomic ratios may be due to the presence of a small amount of W in the samples. The slightly low Ca values are likely an artifact caused by material self-attenuation which is difficult to account for with loose powder samples.

B. Crystal structures of $(\text{Ca}_x\text{Sr}_{2-x})\text{MnWO}_6$

Although the structure of $(\text{Ca}_x\text{Sr}_{2-x})\text{MnWO}_6$ has been determined to be monoclinic, the β angles in the structure of these materials are all very close to 90°, and the lattice parameters a and b are very close to each other, therefore the structure can be considered as pseudo-tetragonal. A trend of

decreasing cell volume against the “ x ” value is observed as expected, as the ionic radius of Ca^{2+} is smaller than that of Sr^{2+} (Shannon, 1976). The WO_6 and MnO_6 octahedra are all distorted, as evidenced from the different W–O distances and Mn–O distances within the octahedra. As the concentration of Ca increases, the average Mn–O distances also decrease from 2.1956 to 2.1923 Å, and W–O distances decrease from 1.9152 to 1.9113 Å.

Figures 2–4 illustrate the 3D structure of $(\text{Ca}_x\text{Sr}_{2-x})\text{MnWO}_6$ featuring alternating distorted MnO_6 and WO_6 octahedra. In brief, the structure is built from corner-shared distorted WO_6 and MnO_6 octahedra similar to the rock salt structure. The most commonly occurring distortion in perovskites is the octahedral tilting (Woodward, 1997). Octahedral tilting is a major contributor to structural variability in perovskites, which refers to the tilting of the BX_6 octahedra about one or more of their symmetry axes, maintaining both regularity of the octahedra (approximately) and their corner connectivity. In other words, such tilting allows greater flexibility in the coordination of the A cation, while leaving the environment of the B cation essentially unchanged. Another octahedral distortion is a rotational mismatch. Rotational mismatch angles can be expressed as torsional angles (consider an arrangement of four atoms A,B,C, and D in a structure, the torsional angle χ [A,B,C,D] is defined by the angle between the planes formed by atoms A,B,C and atoms B,C,D. Viewing along B to C, the torsion angle is considered positive if a clockwise rotation is required to bring atom A in line with atom D). It is obvious that the $(\text{Ca}_x\text{Sr}_{2-x})\text{MnWO}_6$ series exhibits the characteristics of the distorted double perovskite structure, with various rotational

TABLE III. Atomic coordinates and displacement parameters for compounds for $(\text{Ca}_x\text{Sr}_{2-x})\text{MnWO}_6$ ($x = 0.25, 0.5, 0.75, 1.5, 1.75$).

Atom	x	y	z	Site Occ.	U_{iso}	Wyckoff
(1) $(\text{Ca}_{0.25}\text{Sr}_{1.75})\text{MnWO}_6$ ($x = 0.25$)						
Sr1/Ca2	0.996(3)	0.0195(8)	0.250(2)	0.894/0.016	0.0158(7)	4e
Mn3	1/2	0	1/2	1.000	0.0106(8)	2c
W4	1/2	0	0	1.000	0.0097(2)	2d
O5	0.5764(4)	0.0134(3)	−0.26788(7)	1.000	0.0009(14)	4e
O6	0.7251(4)	0.3107(4)	0.0390(3)	1.000	0.0009	4e
O7	0.1879(4)	0.2240(4)	−0.0381(3)	1.000	0.0009	4e
(2) $(\text{Ca}_{0.50}\text{Sr}_{1.50})\text{MnWO}_6$ ($x = 0.5$)						
Sr1/Ca2	1.0001(4)	0.0239(6)	0.2508(9)	0.762/0.238	0.0168(5)	4e
Mn3	1/2	0	1/2	1.000	0.0141(5)	2c
W4	1/2	0	0	1.000	0.0104(2)	2d
O5	0.5773(5)	0.0145(3)	−0.26791(8)	1.000	0.0059(14)	4e
O6	0.7230(4)	0.3132(4)	0.0395(3)	1.000	0.0059	4e
O7	0.1855(4)	0.2216(4)	−0.0386(3)	1.000	0.0059	4e
(3) $(\text{Ca}_{0.75}\text{Sr}_{1.25})\text{MnWO}_6$ ($x = 0.75$)						
Sr1/Ca2	0.987(2)	0.0222(8)	0.2521(9)	0.657/0.343	0.0163(8)	4e
Mn3	1/2	0	1/2	1.000	0.0124(7)	2c
W4	1/2	0	0	1.000	0.0093(2)	2d
O5	0.5793(5)	0.0154(3)	−0.26802(8)	1.000	0.0077(15)	4e
O6	0.7213(4)	0.3150(4)	0.0407(3)	1.000	0.0077	4e
O7	0.1838(4)	0.2199(4)	−0.0396(3)	1.000	0.0077	4e
(4) $(\text{Ca}_{1.50}\text{Sr}_{0.50})\text{MnWO}_6$ ($x = 1.50$)						
Sr1/Ca2	0.0419(6)	−0.0166(15)	0.7519(6)	0.268/0.732	0.0115(9)	4e
Mn3	1/2	0	1/2	1.000	0.0036(7)	2c
W4	1/2	0	0	1.000	0.0089(3)	2d
O5	0.3217(5)	0.2864(5)	0.0455(4)	1.000	0.010(2)	4e
O6	0.2169(5)	0.8212(5)	0.0470(4)	1.000	0.0096	4e
O7	0.0903(5)	0.5203(4)	0.73154(12)	1.000	0.0096	4e
(5) $(\text{Ca}_{1.75}\text{Sr}_{0.25})\text{MnWO}_6$ ($x = 1.75$)						
Sr1/Ca2	0.0488(5)	−0.0172(14)	0.7512(5)	0.120/0.880	0.0120(9)	4e
Mn3	1/2	0	1/2	1.000	0.0055(6)	2c
W4	1/2	0	0	1.000	0.0095(2)	2d
O5	0.3223(5)	0.2872(5)	0.0468(4)	1.000	0.026(2)	4e
O6	0.2171(5)	0.8218(5)	0.0480(4)	1.000	0.026	4e
O7	0.0919(6)	0.5217(5)	0.73158(13)	1.000	0.026	4e

The structure is monoclinic $P2_1/n$ (No. 14). The U_{iso} of O6 and O7 were constrained to be the same as O5.

TABLE IV. Bond distances for $(\text{Ca}_x\text{Sr}_{2-x})\text{MnWO}_6$ ($x = 0.25, 0.5, 0.75, 1.5, 1.75$).

		Bond distances (\AA)				
Atom	Atom	$x = 0.25$	$x = 0.50$	$x = 0.75$	$x = 1.50$	$x = 1.75$
Sr1/Ca2	O5	2.44(2)	2.41(2)	2.468(11)	2.417(3)	2.418(3)
	O5	2.688(6)	2.646(5)	2.661(5)	2.701(4)	2.685(4)
	O5	2.438(2)	2.407(3)	2.468(2)	2.417(6)	2.418(6)
	O5	2.688(2)	2.646(2)	2.661(2)	2.701(7)	2.685(6)
	O6	2.415(2)	2.415(2)	2.345(2)	2.415(3)	2.437(5)
	O6	2.82(2)	2.829(12)	2.799(9)	2.687(4)	2.675(6)
	O6	2.415(11)	2.415(13)	2.345(7)	2.415(6)	2.437(7)
	O6	2.82(2)	2.786(11)	2.812(9)	2.687(6)	2.675(6)
	O7	2.802(12)	2.772(11)	2.812(8)	2.586(9)	2.560(8)
	O7	2.42(2)	2.432(10)	2.383(8)	2.098(5)	2.054(4)
	O7	2.838(11)	2.844(15)	2.800(9)	2.586(2)	2.560(3)
	O7	2.432(2)	2.432(2)	2.382(2)	2.098(3)	2.054(3)
Mn3	Ave	2.601	2.586	2.578	2.484	2.472
	O5 \times 2	2.1896(8)	2.1859(8)	2.1888(8)	2.2026(11)	2.2033(12)
	O6 \times 2	2.1969(7)	2.1971(8)	2.1966(8)	2.1943(11)	2.1929(12)
	O7 \times 2	2.2002(7)	2.2008(8)	2.2009(8)	2.1820(12)	2.1807(13)
	Ave	2.1956	2.1946	2.1954	2.1930	2.1923
W4	O5 \times 2	1.9092(8)	1.9074(8)	1.9078(8)	1.9149(11)	1.9139(12)
	O6 \times 2	1.9193(7)	1.9184(8)	1.9200(8)	1.9207(11)	1.9202(12)
	O7 \times 2	1.9170(7)	1.9163(8)	1.9168(8)	1.9020(12)	1.8997(13)
	Ave	1.9152	1.9140	1.9149	1.9125	1.9113

The structure is monoclinic $P2_1/n$ (No. 14). (Sr/Ca) site has a 12-fold coordination and both Mn and W sites have distorted octahedral 6-fold coordination.

TABLE V. Atomic ratio calculation for Sr/Mn, Ca/Mn, W/Mn, as well as uncertainties from X-ray fluorescence studies.

Sample	Sr/Mn	Ca/Mn	W/Mn
$\text{Sr}_{0.25}\text{Ca}_{1.75}\text{MnWO}_6$	0.28 ± 0.19	1.49 ± 0.19	1.10 ± 0.14
$\text{Sr}_{1.25}\text{Ca}_{0.75}\text{MnWO}_6$	1.39 ± 0.21	0.62 ± 0.11	1.11 ± 0.14
$\text{Sr}_{1.75}\text{Ca}_{0.25}\text{MnWO}_6$	2.10 ± 0.28	0.208 ± 0.036	1.22 ± 0.15

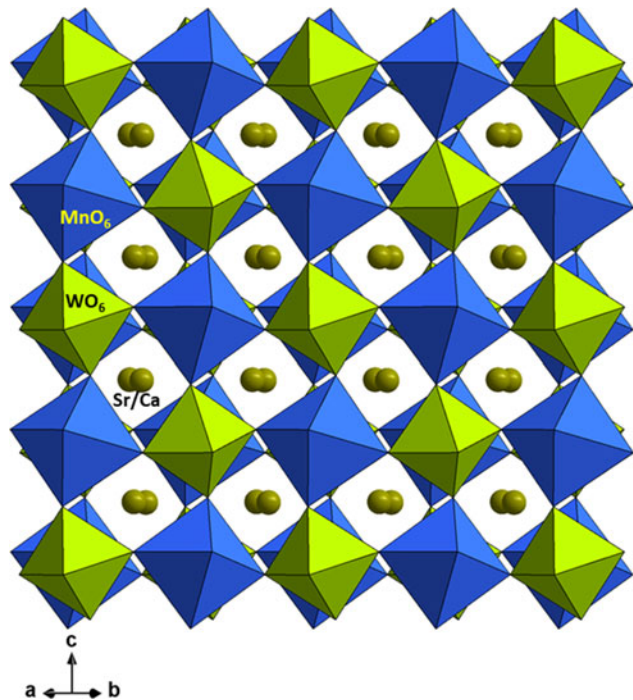


Figure 2. Structure of $(\text{Ca}_x\text{Sr}_{2-x})\text{MnWO}_6$ showing alternating corner-sharing distorted MnO_6 and WO_6 octahedra along ab diagonal to illustrate the distortions of the WO_6 and MnO_6 octahedra. Green – W, blue – Mn, and small spheres – O.

mismatch angles and tilt angles as one views the WO_6 and MnO_6 octahedra with respect to each other (discussed below).

As an example concerning the rotational mismatch angles and tilt angle in the $(\text{Ca}_x\text{Sr}_{2-x})\text{MnWO}_6$ series, Figures 5–8 illustrate the monoclinic structure of $(\text{Sr}_{1.25}\text{Ca}_{0.75})\text{MnWO}_6$ viewing along the c -axis. Figures 5 and 6 give the rotational mismatch angles of the MnO_6 octahedra, view along the c -axis, for two neighboring layers of the monoclinic double perovskite. Figures 7 and 8 (also view along the c -axis) give the rotational mismatch angles of WO_6 octahedra for two neighboring layers. Table VI provides the rotational mismatched angles (given as torsional angles) for five representative compositions of $(\text{Ca}_x\text{Sr}_{2-x})\text{MnWO}_6$ ($x = 0.25, 0.5, 0.75, 1.5, 1.75$), and the tilt angles (Figures 9 and 10). An expected trend is observed. As the Ca content increases (mismatch of the size of Sr and Ca increases) in the Sr/Ca site, the rotational mismatched angles as well as the tilt angles increase. For example, for the MnO_6 octahedra, the mismatched angles are ranged from $7.96(6)^\circ$ to $9.48(8)^\circ$ clockwise, $10.44(6)^\circ$ to $13.12(8)^\circ$ counterclockwise; for the WO_6 octahedra, the mismatched angles are ranged from $9.28(7)^\circ$ to $11.23(9)^\circ$ clockwise, and $11.92(7)^\circ$ to $14.87(9)^\circ$ counterclockwise. Correspondingly, the tilt angles increase from $11.60(15)^\circ$ to $14.20(3)^\circ$ for the MnO_6 octahedra, and from $13.34(2)^\circ$ to $16.35(3)^\circ$ for the WO_6 octahedra.

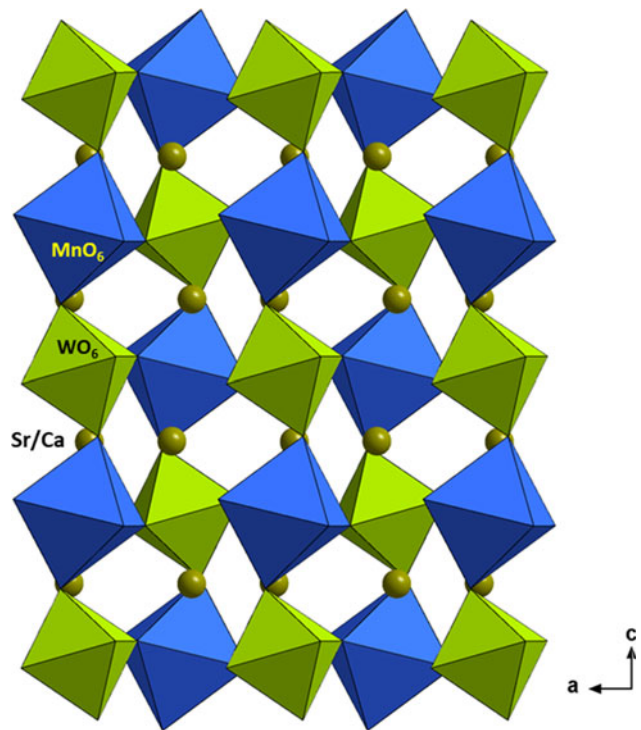


Figure 3. Structure of $(\text{Ca}_x\text{Sr}_{2-x})\text{MnWO}_6$ showing alternating corner-sharing distorted MnO_6 and WO_6 octahedra along the b -axis. Green – W, blue – Mn, and small spheres – O.

The distorted nature of the WO_6 and MnO_6 octahedra are also revealed in the bond distances of Mn–O and W–O, while the bond angles of O–Mn–O and O–W–O are only slightly deviated from 90° or 180° . For example, the W–O distances range from $1.8997(13) \text{ \AA}$ to $1.9207(11) \text{ \AA}$ in WO_6 and from $2.1807(13) \text{ \AA}$ to $2.2033(12) \text{ \AA}$ in MnO_6 .

As shown in Table IV, all Sr/Ca atoms were found to be inside the channels, occupying a 12-oxygen coordination site. The average Sr/Ca–O bond distances range from 2.601 to 2.472 \AA , as the concentration of Ca increases. In general, Ca–O cage would have a smaller coordination number as compared to that of Sr–O and Ba–O containing cages. In this series, because of the doping of Sr on Ca site, the site coordination number of (Ca, Sr) were found to be the same as that of Sr. In other words, the (Ca, Sr)–O cages also have a coordination number of 12, but with a smaller average value of distance of 2.54 \AA . In our previous study of the $(\text{Ba},\text{Sr})\text{CoWO}_6$ series, the coordination for Ba/Sr case was also found to be 12 (Wong-Ng *et al.*, 2020), but the average (Ba,Sr)–O distance is at a larger value of 2.82 \AA .

C. Bandgap studies

Figure 11 shows the UV–visible absorption spectra of the $(\text{Ca}_x\text{Sr}_{2-x})\text{MnWO}_6$ ($x = 0.0, 0.25, 0.5, 0.75, 1.25, 1.5, 1.75$) compounds. There is a strong absorption between 500 and 700 nm for all samples. The absorption edge varies with the Ca/Sr ratio and a strong red-shift was observed in these $(\text{Ca}_x\text{Sr}_{2-x})\text{MnWO}_6$ samples.

The optical bandgaps E_g can be estimated from the absorption coefficient (α) using the Tauc relation (Tauc *et al.*, 1966),

$$\alpha h\nu = A(h\nu - E_g)^n$$

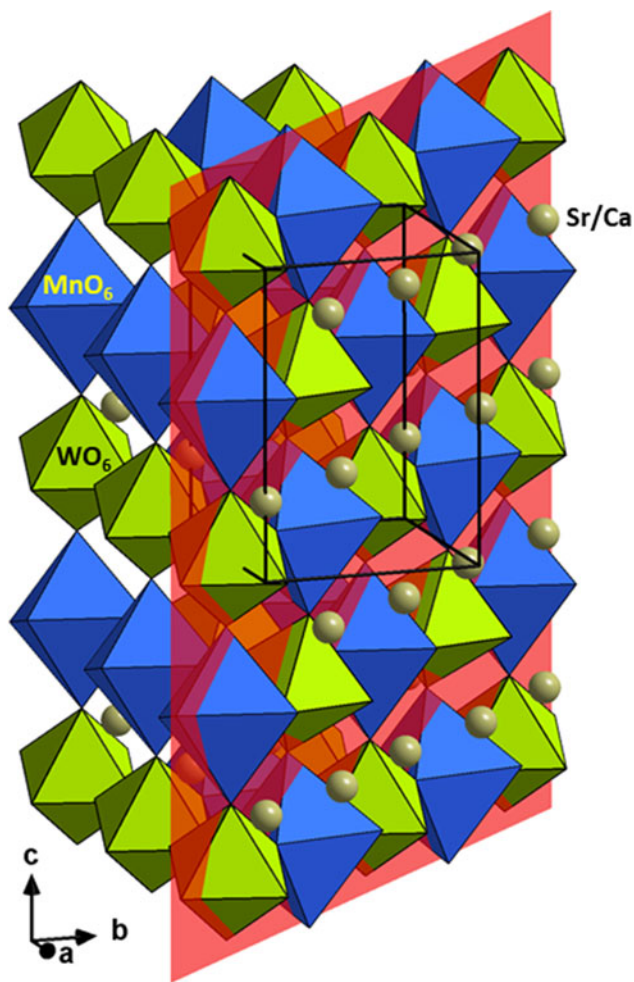


Figure 4. Structure of $(\text{Ca}_x\text{Sr}_{2-x})\text{MnWO}_6$ with an inserted plane as a reference to show the relative size of the MnO_6 and WO_6 octahedra and the 3D structure more clearly.

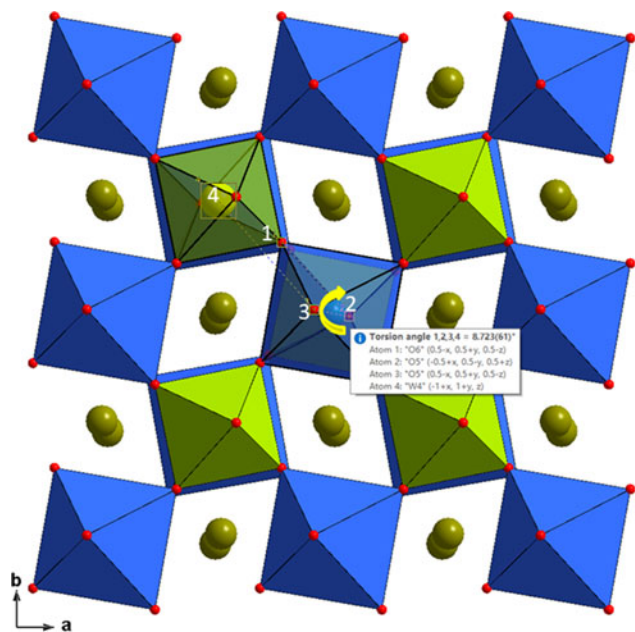


Figure 5. Rotational mismatch angles (see definition in the legend of Table VI) of MnO_6 octahedron (blue) for the monoclinic double perovskite $(\text{Sr}_{1.25}\text{Ca}_{0.75})\text{MnWO}_6$, viewed approximately along the c -axis.

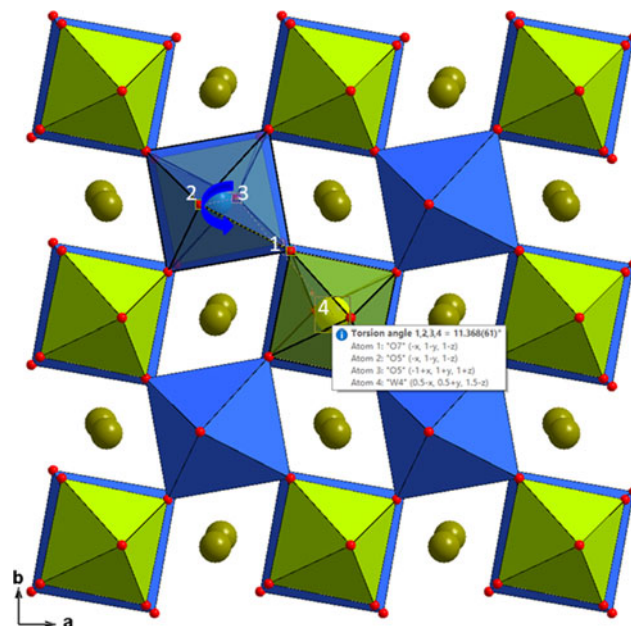


Figure 6. Rotational mismatch angles (see definition in the legend of Table VI) of the next layer of MnO_6 octahedron (blue) for the monoclinic double perovskite $(\text{Sr}_{1.25}\text{Ca}_{0.75})\text{MnWO}_6$, viewed approximately along the c -axis.

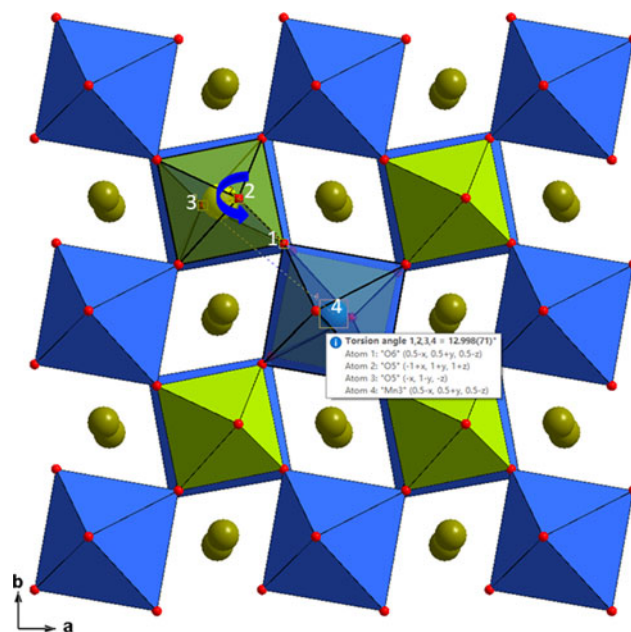


Figure 7. Rotational mismatch angles (see definition in the legend of Table VI) of WO_6 octahedron (green) for the monoclinic double perovskite $(\text{Sr}_{1.25}\text{Ca}_{0.75})\text{MnWO}_6$, viewed approximately along the c -axis.

where A is a constant that depends on the transition probability, $h\nu$ is the energy of incident photons, n is an index that characterizes the optical absorption process. A linear fitting near the absorption edge can be achieved in the $(\alpha h\nu)^{1/n}$ vs. $h\nu$ plot to calculate the bandgap of these semiconductor materials. The values of $n=2$, $1/2$, 3 , and $3/2$ correspond to allowed-indirect, allowed-direct, forbidden-indirect, and forbidden-direct bandgap, respectively (Qasrawi, 2005). The UV–visible spectra shown in Figure 11 were fitted with

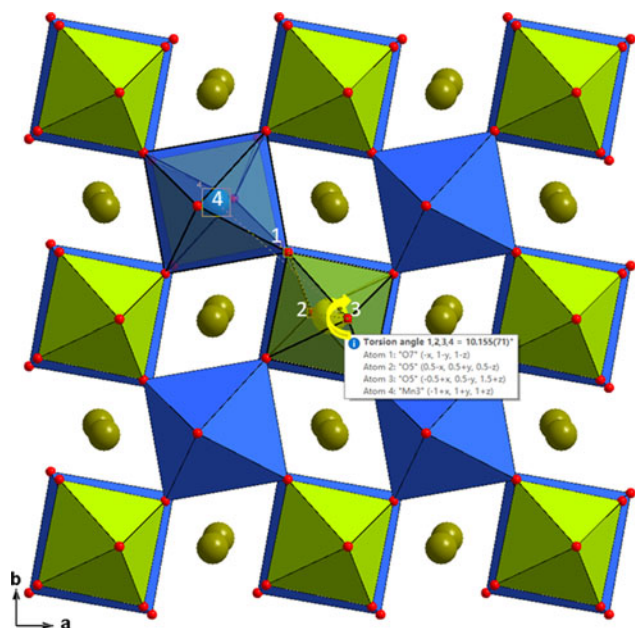


Figure 8. Rotational mismatch angles (see definition in the legend of Table VI) of the next layer of WO_6 octahedron (green) for the monoclinic double perovskite $(\text{Sr}_{1.25}\text{Ca}_{0.75})\text{MnWO}_6$, viewed approximately along the c -axis.

$n = 1/2, 2, 3$, and $3/2$ based on the Tauc relation. We found that the value of $n = 1/2$ fitted the curves best. Figure 12 shows the Tauc plots of the samples when $n = 1/2$. Therefore, the synthesized compound appears to be a direct-allowed

TABLE VI. Rotational mismatched angles (torsional angles) and tilt angles found in $(\text{Ca}_x\text{Sr}_{2-x})\text{MnWO}_6$ ($x = 0.25, 0.5, 1.5, 1.75$). The tilt angles of WO_6 .

x	Octahedron	Direction of rotation	Torsional angles ($^\circ$)	Tilt angles ($^\circ$)
0.25	MnO_6	Clockwise	7.96(6)	11.60(15)
		Counter-clockwise	10.44(6)	
	WO_6	Clockwise	9.28(7)	13.34(2)
		Counter-clockwise	11.92(7)	
0.5	MnO_6	Clockwise	8.42(6)	11.77(2)
		Counter-clockwise	10.96(6)	
	WO_6	Clockwise	9.83(7)	13.52(2)
		Counter-clockwise	12.51(7)	
0.75	MnO_6	Clockwise	8.72(6)	12.07(2)
		Counter-clockwise	11.37(6)	
	WO_6	Clockwise	10.16(7)	13.88(2)
		Counter-clockwise	13.00(7)	
1.5	MnO_6	Clockwise	9.48(8)	13.89(3)
		Counter-clockwise	12.91(8)	
	WO_6	Clockwise	11.12(9)	15.98(3)
		Counter-clockwise	14.72(9)	
1.75	MnO_6	Clockwise	9.48(8)	14.20(3)
		Counter-clockwise	13.12(8)	
	WO_6	Clockwise	11.23(9)	16.35(3)
		Counter-clockwise	14.87(9)	

Rotational mismatch angles can be expressed as torsional angles (consider an arrangement of four atoms A,B,C, and D in a structure, the torsional angle χ [A,B,C,D] is defined by the angle between the planes formed by atoms A,B,C and atoms B,C,D. Viewing along B to C, the torsion angle is considered positive if a clockwise rotation is required to bring atom A in line with atom D). The tilt angles of WO_6 and MnO_6 octahedra are referred to the (Mn–W–O) and the (W–Mn–O) angles, respectively.

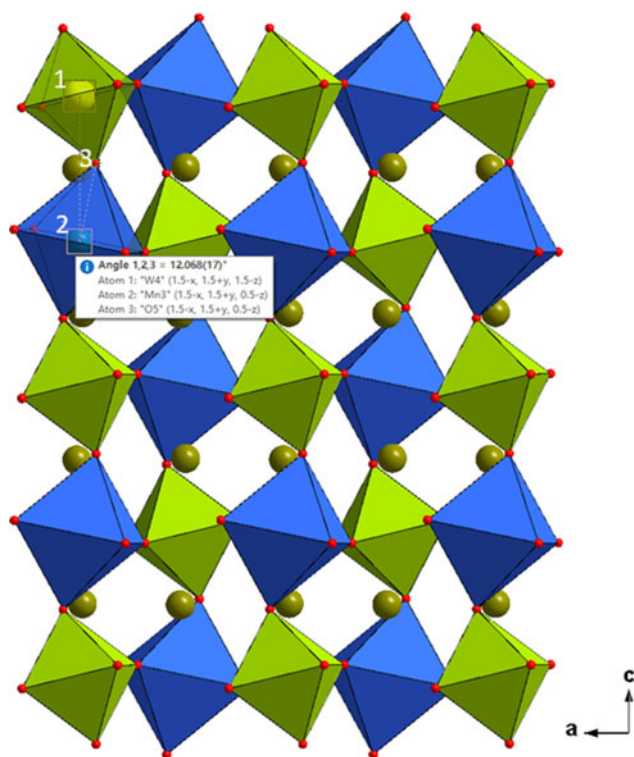


Figure 9. Tilt angles of MnO_6 octahedron (W–Mn–O) (blue) for the monoclinic double perovskite $(\text{Sr}_{1.25}\text{Ca}_{0.75})\text{MnWO}_6$, viewed along the b -axis.

semiconductor. The bandgaps were then calculated based on $n = 1/2$. In other words, the bandgaps E_g of the $(\text{Ca}_x\text{Sr}_{2-x})\text{MnWO}_6$ ($x = 0.0, 0.25, 0.5, 0.75, 1.00, 1.25, 1.5, 1.75, 2.0$) compounds were obtained by extrapolating the linear portion

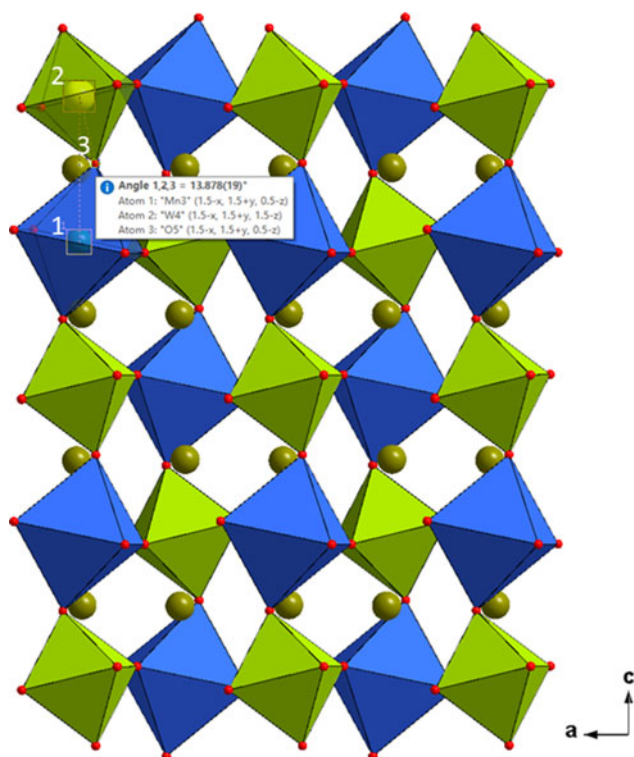


Figure 10. Tilt angles of WO_6 octahedron (Mn–W–O) (green) for the monoclinic double perovskite $(\text{Sr}_{1.25}\text{Ca}_{0.75})\text{MnWO}_6$, viewed along the b -axis.

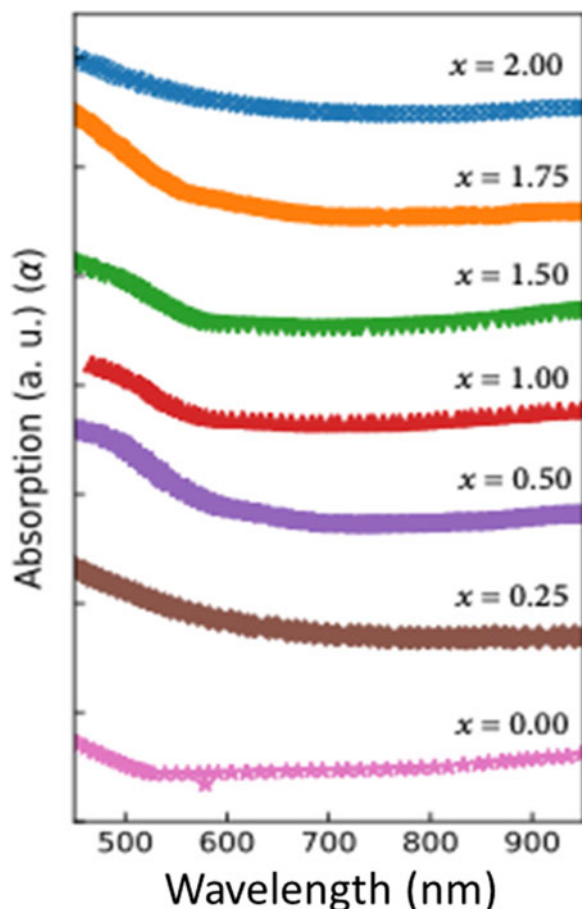


Figure 11. UV-visible absorption spectra of the as-synthesized $(\text{Ca}_x\text{Sr}_{2-x})\text{MnWO}_6$ ($x = 0.25, 0.5, 0.75, 1.25, 1.5, 1.75$) compounds.

of the plots of $(\alpha h\nu)^2$ vs. photon energy $h\nu$ ($(\alpha h\nu)^2 = 0$), as shown in Figure 12.

Figure 13 shows the calculated bandgap of $(\text{Ca}_x\text{Sr}_{2-x})\text{MnWO}_6$. The bandgap values (allowed-direct electronic transitions) are lowest ($E_g = 1.68$ eV) when $x = 1.00$ and the highest when $x = 0$ ($E_g = 2.28$ eV) and $x = 2.00$ ($E_g = 2.30$ eV). The crystallographic structure and Ca/Sr ratio clearly affect the bandgap value. Theoretical calculation indicated that the bandgap of monoclinic Ca_2MnWO_6 (space group of $P2_1/c$) to be 2.199 eV (Persson, 2014a). The theoretical bandgap value of monoclinic Sr_2MnWO_6 (space group of $P2_1/c$) was reported as 1.945 eV (Persson, 2014b). Both calculated values are somewhat lower than our values, but still greater than those values of compounds with intermediate x values. Additionally, the bandgap of the monoclinic phase was calculated to be of the “indirect” type (different from our estimated bandgap of the “direct” type). The bandgap of trigonal Ca_2MnWO_6 (space group of $R3$) was calculated to be 2.679 eV (Jain *et al.*, 2013) by assuming an indirect-bandgap. The bandgap of cubic Sr_2MnWO_6 was experimentally estimated to be 2.5 eV using reflectance spectroscopy measurements (Fujioka *et al.*, 2004), 9.6% higher than our value. Regardless, all these reported values and our measured values are not substantially different, and they are all nominally under 2.7 eV.

From the above UV-visible absorption and bandgap data, it is clear that the $(\text{Ca}_x\text{Sr}_{2-x})\text{MnWO}_6$ series can absorb visible light of the solar radiation. Therefore, the $(\text{Ca}_x\text{Sr}_{2-x})\text{MnWO}_6$ materials are potential photocatalysts and photovoltaic materials.

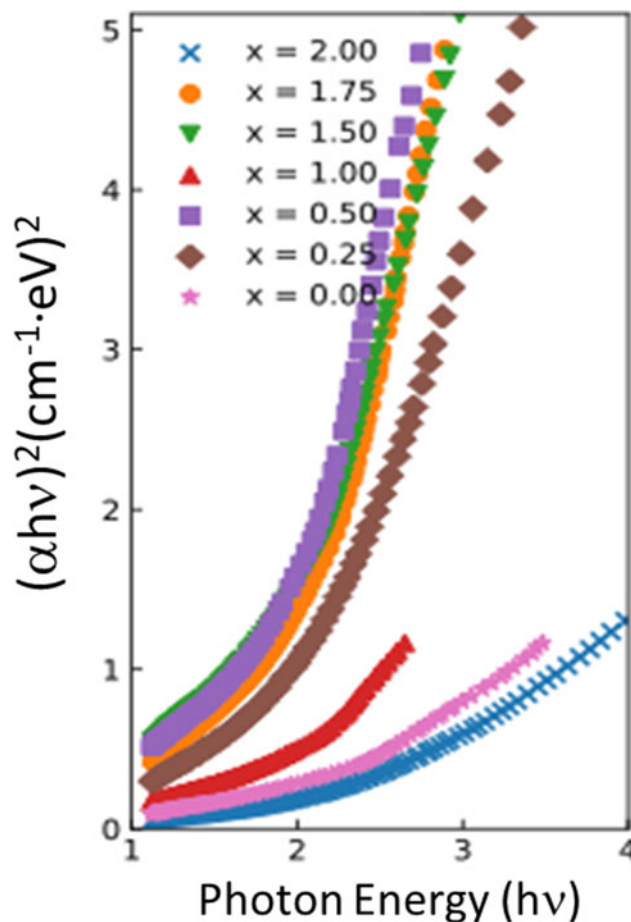


Figure 12. Tauc plot for calculating bandgaps E_g of $(\text{Ca}_x\text{Sr}_{2-x})\text{MnWO}_6$ ($x = 0.25, 0.5, 0.75, 1.25, 1.5, 1.75$) by extrapolation of the linear portion of the plots of $(\alpha h\nu)^2$ vs. photon energy $h\nu$.

D. Reference powder X-ray diffraction patterns

Reference patterns for the $(\text{Ca}_x\text{Sr}_{2-x})\text{MnWO}_6$ ($x = 0.25, 0.5, 0.75, 1.5, 1.75$) compounds have been prepared and submitted for inclusion in the PDF. An example of the pattern $(\text{Ca}_{0.5}\text{Sr}_{1.5})\text{MnWO}_6$ (with d -spacing values >0.8 Å) is given

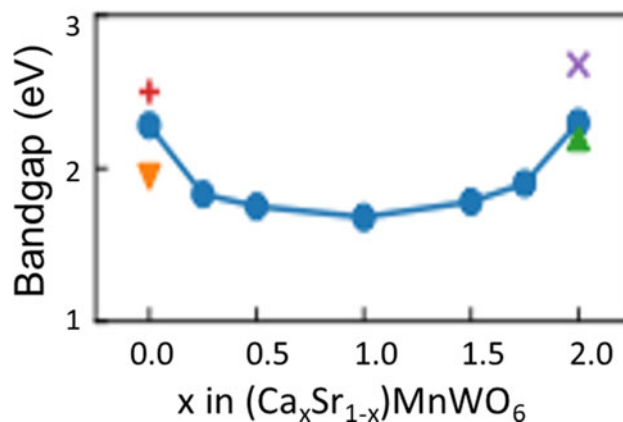


Figure 13. Bandgap values of $(\text{Ca}_x\text{Sr}_{2-x})\text{MnWO}_6$. Reported values are also listed for comparison. x : theoretical value of a rhombohedral phase with $R3$ space group (Jain *et al.*, 2013); $+$: experimental values of a cubic phase with space group of $Fm\bar{3}m$ (Fujioka *et al.*, 2004); upward triangle: theoretical value of monoclinic $P2_1/c$ structure (Persson, 2014a); downward triangle: theoretical value of monoclinic $P2_1/c$ structure (Persson, 2014b).

TABLE VII. X-ray powder pattern for (Ca_{0.50}Sr_{1.5})MnWO₆.

d_{cal}	I_{obs}	h	k	l		d_{cal}	I_{obs}	h	k	l	
4.6002	289	1	0	1	M	4.6002	289	1	0	-1	M
4.5352	286	0	1	1		3.9561	423	1	1	9	M
3.9561	423	0	0	2	M	3.5402	7	1	1	1	M
3.5402	7	1	1	-1	M	2.8318	226	2	0	0	
2.7957	999	1	1	2	M	2.7957	999	1	1	-2	M
2.7706	258	0	2	0		2.4024	95	2	1	1	M
2.4024	95	2	1	-1	M	2.3877	74	1	0	3	
2.3742	158	1	2	-1	+	2.3009	18	2	0	2	M
2.3009	18	2	0	-2	M	2.2676	12	0	2	2	
2.1916	7	1	1	3	M	2.1916	7	1	1	-3	M
2.1245	3	2	1	2	M	2.1245	3	2	1	-2	M
2.1051	4	1	2	2	M	2.1051	4	1	2	-2	M
1.9804	306	2	2	0		1.9733	174	0	0	4	
1.9209	4	2	2	1	M	1.9209	4	2	2	-1	M
1.8354	33	3	0	-1		1.8198	48	2	1	3	M
1.8198	48	2	1	-3	M	1.8082	48	1	2	3	M
1.8082	48	1	2	-3	M	1.7985	26	0	3	1	
1.7870	55	3	1	0		1.7665	181	2	2	-2	+
1.7560	54	1	3	0		1.6279	248	3	1	2	M
1.6279	248	3	1	-2	M	1.6192	126	2	0	4	M
1.6192	126	2	0	-4	M	1.6054	417	0	2	4	+
1.5351	21	3	0	3		1.5301	55	3	2	-1	
1.5188	94	2	3	1	+	1.5118	14	0	3	3	
1.4794	2		3	1	3	1.4159	40	4	0	0	
1.3979	205	2	2	4	M	1.3979	205	2	2	-4	M
1.3853	49	0	4	0		1.3519	32	4	1	1	
1.3427	45	3	2	3		1.3383	31	2	1	5	M
1.3383	31	2	1	-5	M	1.3329	92	1	2	-5	+
1.3254	75	3	1	4	+	1.3203	15	3	3	0	
1.3118	40	1	3	4	M	1.3118	40	1	3	4	M
1.3071	13	0	4	2		1.2608	48	4	2	0	
1.2521	101	3	3	2	M	1.2521	101	3	3	2	M
1.2485	120	1	1	6	M	1.2485	120	1	1	-6	M
1.2444	58	2	4	0		1.2156	21	4	1	-3	
1.2101	14	3	0	-5		1.2008	52	4	2	2	+
1.1982	15	1	4	3		1.1931	12	2	0	6	M
1.1931	12	2	0	-6	M	1.1872	36	2	4	2	+
1.1504	38	4	0	4	M	1.1504	38	4	0	-4	M
1.1338	50	0	4	4		1.1210	10	5	0	-1	
1.1127	12	4	3	1		1.1093	29	5	1	0	M
1.1093	29	3	2	-5	M	1.1057	37	3	4	-1	+
1.0968	43	3	3	-4	+	1.0876	7	1	5	0	
1.0683	48	5	1	2	M	1.0683	48	5	1	-2	M
1.0607	114	3	1	6	+	1.0527	132	2	4	4	+
1.0485	56	1	5	2	M	1.0485	56	1	5	-2	M
1.0410	8	5	0	3		1.0396	14	5	2	-1	
1.0363	12	4	1	5		1.0329	13	4	3	-3	
1.0286	21	2	1	-7	M	1.0286	21	3	4	3	M
1.0271	11	1	1	7	M	1.0271	11	1	1	-7	M
1.0237	15	1	4	-5	M	1.0237	15	2	5	1	M
0.9902	19	4	4	0		0.9867	13	0	0	8	
0.9745	12	5	2	3		0.9682	12	3	0	7	M
0.9682	12	5	1	4	M	0.9653	33	5	3	0	+
0.9604	28	4	4	2	+	0.9575	13	1	1	8	M
0.9575	13	1	1	-8	M	0.9557	10	3	5	0	.
0.9525	12	1	5	4	M	0.9525	12	1	5	-4	M
0.9379	41	5	3	2	M	0.9379	41	5	3	-2	M
0.9319	70	3	3	-6	+	0.9291	72	0	2	8	+
0.9239	21	6	1	1	M	0.9239	21	0	6	0	M
0.9180	14	6	0	2	M	0.9180	14	6	0	-2	M
0.9160	5		4	3	5	0.9145	11	3	2	7	
0.9111	18	3	4	-5	M	0.9111	18	4	2	6	M
0.9096	8		4	2	-6	0.9055	5		1	6	-1
0.9040	11	2	4	6	M	0.9040	11	2	4	-6	M
0.8992	5	0	6	2		0.8935	9	6	2	0	
0.8850	40	4	4	4	M	0.8850	40	4	4	-4	M

Continued

TABLE VII. Continued

d_{cal}	I_{obs}	h	k	l		d_{cal}	I_{obs}	h	k	l	
0.8831	36	2	2	8	M	0.8831	36	2	2	−8	M
0.8780	16	2	6	0		0.8768	10	6	1	−3	
0.8728	7	5	2	−5		0.8713	36	6	2	2	+
0.8674	23	5	3	−4	+	0.8643	6	3	1	8	
0.8602	12	3	5	4	M	0.8602	12	3	5	−4	M
0.8510	5	6	0	−4		0.8489	12	5	1	6	
0.8476	13	5	1	−6		0.8382	30	1	5	6	M
0.8382	30	1	5	−6	M	0.8363	26	0	6	4	M
0.8363	26	6	3	1	M	0.8322	8	5	4	3	
0.8284	10	2	1	9	M	0.8284	10	4	5	−3	M
0.8270	5	1	2	−9		0.8250	7	3	6	−1	
0.8140	15	6	2	4	M	0.8140	15	6	2	−4	M
0.8095	11	4	0	8	M	0.8095	11	4	0	−8	M
0.8031	27	0	4	8	M	0.8031	27	2	6	4	M
0.8021	18	6	1	5	M	0.8021	18	2	6	−4	M
0.8005	15	7	1	0	M	0.8005	15	6	3	−3	M

The structure is monoclinic $P2_1/n$ (No. 14). The symbols “M” and “+” refer to peaks containing contributions from two and more than two reflections, respectively. The particular peak that has the strongest intensity in the entire pattern is assigned an intensity of 999 and other lines are scaled relative to this value. The d -spacing values are calculated values from refined lattice parameters, and “I” represents integrated intensity values.

in Table VII. In this pattern, the symbols “M” and “+” refer to peaks containing contributions from two and more than two reflections, respectively. The particular peak that has the strongest intensity in the entire pattern is assigned an intensity of 999 and other lines are scaled relative to this value. The d -spacing values are calculated values from refined lattice parameters. The intensity values reported are integrated intensities (rather than peak heights). For resolved overlapped peaks, intensity-weighted calculated d -spacing, along with the observed integrated intensity and the hkl indices of both peaks (for “M”), or the hkl indices of the strongest peak (for “+”) are used. For peaks that are not resolved at the instrumental resolution, the intensity-weighted average d -spacing and the summed integrated intensity value are used. In the case of a cluster, unconstrained profile fits often reveal the presence of multiple peaks, even when they are closer than the instrumental resolution. In this situation, both d -spacing and intensity values are reported independently.

IV. SUMMARY AND FUTURE WORK

We have successfully determined the structure, measured the bandgap and prepared X-ray powder diffraction patterns for the series of semiconductors $(\text{Ca}_x\text{Sr}_{2-x})\text{MnWO}_6$. Their X-ray patterns have been submitted to the ICDD for inclusion in the PDF database. All Sr/Ca sites have 12-fold coordination environment and all the ordered W and Mn sites are 6-fold (octahedral) coordinated. These double perovskites consist of alternate distorted MnO_6 and WO_6 octahedra along the c -axis. These octahedra are rotated and tilted with respect to each other along the pseudo-tetragonal c -axis. The bandgaps of these samples including literature reported values are all less than 2.7 eV (whether experimental or theoretical values), therefore $(\text{Ca}_x\text{Sr}_{2-x})\text{MnWO}_6$ can absorb visible light of the solar radiation and they are potential photocatalysts and photovoltaic materials. We plan to continue studying selected members of the $(\text{Ca}_x\text{Sr}_{2-x})\text{MnWO}_6$ series for their magnetic structures by using neutron diffraction and density function (DFT) calculations.

ACKNOWLEDGEMENTS

ICDD is acknowledged for the Grants-in-Aid assistance for the project (Grant #0903).

CONFLICTS OF INTEREST

The authors declare none.

- Blasse, G. (1965). “Some magnetic properties of mixed metal oxides with ordered perovskite structure,” *Philips Res. Rep.* **20**, 327.
- Fujioka, F., Frantti, J., and Kakihana, M. (2004). “Franck-Condon modes in Sr_2MnWO_6 double perovskite,” *J. Phys. Chem. B* **108**, 17012–17014.
- Galasso, F. (1969). *Structure, Properties and Preparation of Perovskite-Type Compounds* (Pergamon Press, Oxford).
- Gates-Rector, S. D. and Blanton, T. N. (2019). “The Powder Diffraction File: a quality materials characterization database,” *Powder Diffr.* **34**, 352–360.
- Jain, A., Ong, S. P., Hautier, G., Chen, W., Richards, W. D., Dacek, S., Cholia, S., Gunter, D., Skinner, D., Ceder, G., and Persson, K. A. (2013). “The materials project: a materials genome approach to accelerating materials innovation,” *APL Mater.* **1**, 011002.
- Manoun, B., Ezzahi, A., Benmokhtar, S., Bihe, L., Tamraoui, Y., Haloui, R., Mirinioui, F., Addakiri, S., Igartua, J. M., and Lazor, P. (2013). “X-ray diffraction and Raman spectroscopy studies of temperature and composition induced phase transitions in $\text{Ba}_{2-x}\text{Sr}_x\text{MWO}_6$ ($\text{M} = \text{Ni}, \text{Co}$ and $0 \leq x \leq 2$) double perovskite oxides,” *J. Mol. Struct.* **1045**, 1–14.
- Persson, K. (2014a). “Materials Data on Ca_2MnWO_6 (SG:14) by Materials Project”, sponsored by USDOE Office of Science (SC), Basic Energy Sciences (BES). doi:10.17188/1194235.
- Persson, K. (2014b). “Materials Data on Sr_2MnWO_6 (SG:14) by Materials Project”, sponsored by USDOE Office of Science (SC), Basic Energy Sciences (BES). doi:10.17188/1194235.
- Qasrawi, A. F. (2005). “Refractive index, band gap and oscillator parameters of amorphous GaSe thin films,” *Cryst. Res. Technol.* **40**(6), 610–614.
- Rietveld, H. M. (1969). “A profile refinement method for nuclear and magnetic structures,” *J. Appl. Crystallogr.* **2**, 65–71.
- Shannon, R. D. (1976). “Revised effective ionic radii and systematic studies of interatomic distances in halides and chalcogenides,” *Acta Crystallogr., Sect. A: Cryst. Phys., Diff., Theor. Gen. Crystallogr.* **32**, 751–767.
- Tauc, J., Grigorovici, R., and Vancu, A. (1966). “Optical properties and electronic structure of amorphous germanium,” *Phys. Status Solidi B* **15**(2), 627–637.
- Toby, B. H. and Von Dreele, R. B. (2013). “GSAS-II: the genesis of a modern open-source all purpose crystallography software package,” *J. Appl. Crystallogr.* **46**(2), 544–549.

- Tritt, T. M. (1996). "Thermoelectrics run hot and cold," *Science* **272**, 1276–1277.
- Viola, M. C., Martínez-Lope, M. J., Alonso, J. A., Martínez, J. L., De Paoli, J. M., Pagola, S., Pedregosa, J. C., Fernández-Díaz, M. T., and Carbonio, R. E. (2003). "Structure and magnetic properties of Sr_2CoWO_6 : an ordered double perovskite containing $\text{Co}^{2+}(\text{HS})$ with unquenched orbital magnetic moment," *Chem. Mater.* **15**(8), 1655–1663.
- Wong-Ng, W., Liu, G., Yang, Y. Q., Derbeshi, R., Windover, D., and Kaduk, J. A. (2020). "Crystal chemistry, X-ray diffraction reference patterns, and band gap studies for $(\text{Ba}_x\text{Sr}_{1-x})_2\text{CoWO}_6$ ($x = 0.1, 0.2, 0.3, 0.5, 0.7, 0.9$)," *Powder Diffr.* **35**(3), 197–205.
- Woodward, P. M. (1997). "Octahedral tilting in perovskites. I. Geometrical considerations," *Acta Crystallogr., Sect. B: Struct. Sci.* **53**, 32–43.
- Zhao, F., Yue, Z. X., Gui, Z. L., and Li, L. T. (2005). "Preparation, characterization and microwave dielectric properties of A_2BWO_6 ($\text{A} = \text{Sr}, \text{Ba}$; $\text{B} = \text{Co}, \text{Ni}, \text{Zn}$) double perovskite ceramics," *Jpn. J. Appl. Phys.* **44**, 8066.